

Hydrodynamic helicity polarization in relativistic heavy ion collisions

Cong Yi* and Shi Pu†

Department of Modern Physics, University of Science and Technology of China, Hefei, Anhui 230026, China

Jian-Hua Gao‡

Shandong Provincial Key Laboratory of Optical Astronomy and Solar-Terrestrial Environment, Institute of Space Sciences, Shandong University, Weihai, Shandong 264209, China

Di-Lun Yang§

Institute of Physics, Academia Sinica, Taipei, 11529, Taiwan

Abstract

We study helicity polarization through the (3+1) dimensional relativistic viscous hydrodynamic models at $\sqrt{s_{NN}} = 200\text{GeV}$ Au+Au collisions. Similar to the local spin polarization, we consider the helicity polarization beyond global equilibrium and investigate the contributions induced by thermal vorticity, shear viscous tensor, and the fluid acceleration. We find that the local helicity polarization induced by thermal vorticity dominates over other contributions. It also implies that in the low-energy collisions, the the fluid vorticity as part of thermal vorticity may play the crucial role to the total helicity polarization. Such a finding could be useful for probing the local strength of vorticity in rotational quark gluon plasmas by measuring helicity polarization. Our simulation confirms the strict space reversal symmetry, whereas we also compare our numerical results with approximated relations derived from ideal Bjorken flow. Our studies also provide a baseline for the future investigation on local parity violation through the correlations of helicity polarization.

*Electronic address: congyi@mail.ustc.edu.cn

†Electronic address: shipu@ustc.edu.cn

‡Electronic address: gaojh@sdu.edu.cn

§Electronic address: dlyang@gate.sinica.edu.tw

I. INTRODUCTION

In non-central heavy-ion collisions, large orbital angular momentum (OAM) of the order of $10^5\hbar$ is produced, part of which transfers into quark gluon plasma (QGP) as the form of vortical fields. The large OAM is deposited in the QGP with fast rotation. Such rotation can lead to the spin polarization of the hadrons similar to the famous Barnett effect [1]. The global polarization of Λ and $\bar{\Lambda}$ hyperons created in relativistic heavy ion collisions through spin-orbital coupling was first proposed by Liang and Wang in Refs. [2, 3]. In 2017, the STAR collaboration observed the global polarization of Λ hyperons [4]. There are many theoretical approaches to investigate the global polarization including the pioneer works based on the statistical field theory [5–7] and Wigner-function approach near equilibrium [8], as theoretical predictions even before experimental measurements, from which the derived modified Cooper-Frye formula paves the way for numerical simulations. In light of this formula, the results from numerical simulations [9–18] are consistent with the experimental measurements for the global polarization. See also Refs. [19–25] for recent studies of the spin polarization in low-energy collisions.

Later, in order to study the structure of the local vorticity in the QGP, STAR collaboration measures the local spin polarization of Λ hyperons as a function of azimuthal angle along the global angular momentum and the beam directions [26, 27], dubbed as the transverse and longitudinal polarization. Surprisingly, the numerical simulations from the same models mentioned above for the global polarizations, disagree with the experiment data. See the disagreements in e.g. relativistic hydrodynamics [16, 28] and transport models [10, 14, 29]. For longitudinal polarization, these theoretical calculations obtain the results with qualitatively an opposite sign compared to experimental observations. This discrepancy is called the “sign” problem for spin polarization in relativistic heavy-ion collisions. It is found in Refs. [30–32] that the feed-down effect cannot explain this disagreement either. Although some phenomenological models [33–36] qualitatively describe the experimental data, the “sign” problem is still an open question in the community.

Nevertheless, most of the theoretical studies have assumed that the spin degree of freedom is in global thermal equilibrium at a freezeout hypersurface, which is actually not justified from the first principle. A lot of efforts are made to investigate dynamical spin polarization with non-equilibrium effects both from macroscopic and microscopic approaches. One of

the macroscopic theories is relativistic spin hydrodynamics [37–65], which includes the spin degree of freedom and spin-orbit interaction by coupling the hydrodynamic equations with the conservation of angular momentum. On the other hand, one of the microscopic descriptions that complements the macroscopic approach is the quantum kinetic theory (QKT) for massive fermions with collisions [66–78], which is an extension of the chiral kinetic theory (CKT) for massless fermions [79–97]. Also see Ref. [98] for a recent review of QKT. There is also a distinct microscopic model incorporating the spin-orbital interaction in collisions in Ref. [99]. In addition, there have been further studies on the QKT for polarized photons [100–102] with possible generalization to weakly coupled gluons and the inclusion of background chromo-electromagnetic fields for the QKT of massless and massive fermions [103–105].

Recently, the shear induced polarization, which was found for massless fermions in Ref. [88] and later obtained for massive fermions [106–108] in local thermal equilibrium, has drawn lots of attentions. Including such an effect, the local spin polarization from numerical simulations could qualitatively match the experimental observations [109, 110], while the numerical results depend on different approximations adopted. It is also pointed out that the polarization of strange quarks is sensitive to the equation of state and other parameters [111, 112]. See also Ref. [113] for similar studies on the parameter dependences in the $\sqrt{s_{NN}} = 19.6\text{GeV}$ collisions and Refs. [58, 112, 114, 115] for related studies. Therefore, solving the “sign” problem requires more systematic studies on the off-equilibrium effects, which may be obtained from spin hydrodynamics or QKT.

Moreover, helicity polarization defined as the local spin polarization projected to the momentum direction of polarized hadrons has been proposed in Refs. [116, 117], which could be implemented to probe local parity violation characterized by an axial chemical potential in quantum chromodynamics (QCD) matter at finite temperature (see Ref. [104] for a different proposal) to complement the longstanding search for the chiral magnetic effect [118–123]. See also Refs. [124–127] for other studies and phenomenological applications related to particle helicity in relativistic heavy ion collisions. In order to extract the signal of local-parity violation from helicity-helicity (polarization) correlations [116, 117], it is essential to study the helicity polarization without an axial chemical potential from hydrodynamic as a baseline for the future analysis.

In this work, we study the hydrodynamic helicity polarization. We focus on the local-

equilibrium contributions from thermal vorticity, shear corrections, and fluid acceleration and analyze their features analytically. Then, we implement the (3+1)-dimensional relativistic viscous hydrodynamic models to simulate the hydrodynamic helicity polarization. We examine the relations derived from the ideal Bjorken flow [117] and space reversal symmetry. We also investigate the helicity polarization for both Λ -hyperon equilibrium and strange-quark equilibrium (abbreviated as Λ equilibrium and s equilibrium) scenarios proposed in Refs. [109, 111].

The structure of this article is as follows. In Sec. II, we introduce the helicity polarization with corrections in local equilibrium [88, 111] and briefly review the analysis of the contribution from thermal vorticity based on symmetries [116, 117]. In Sec. III, we implement the (3+1)dimensional viscous hydrodynamic simulation to study the azimuthal angle and the momentum rapidity dependence of helicity polarization. At last, we summarize our results and make further discussions in Sec. IV. Throughout this work, we adopt the metric $g_{\mu\nu} = \text{diag}\{+, -, -, -\}$, $\epsilon^{0123} = 1$ and the projector $\Delta^{\mu\nu} = g^{\mu\nu} - u^\mu u^\nu$ with u^μ being fluid velocity. We also use the boldface notation such as \mathbf{k} to denote the spatial component of a four-vector like k^μ .

II. HELICITY POLARIZATION

In this section, we briefly review the formalism for helicity polarization based on Ref. [28, 116, 117]. For simplicity, we concentrate on the helicity polarization induced by hydrodynamic variables and neglect the contribution from axial chemical potential.

We start from the single-particle mean spin vector $\mathcal{S}^\mu(p)$ by the modified Cooper-Frye formula [7, 128].

$$\mathcal{S}^\mu(p) = \frac{\int d\Sigma \cdot p \mathcal{J}_5^\mu(p, X)}{2m_\Lambda \int d\Sigma \cdot \mathcal{N}(p, X)}, \quad (1)$$

where the m_Λ is the mass of Λ hyperons, Σ_μ is the normal vector of the freeze-out surface, the $\mathcal{N}^\mu(p, X)$ and $\mathcal{J}_5^\mu(p, X)$ are number density and axial-charge current density in phase space, respectively. The $\mathcal{N}^\mu(p, X)$ and $\mathcal{J}_5^\mu(p, X)$ can be derived from the quantum kinetic theory [91]

$$\begin{aligned} \mathcal{N}^\mu(p, X) &= 2 \int_{p \cdot n} [\mathcal{J}_+^\mu(p, X) + \mathcal{J}_-^\mu(p, X)], \\ \mathcal{J}_5^\mu(p, X) &= 2 \int_{p \cdot n} [\mathcal{J}_+^\mu(p, X) - \mathcal{J}_-^\mu(p, X)], \end{aligned} \quad (2)$$

where $\int_{p \cdot n} \equiv \int dp \cdot np \cdot n \theta(p \cdot n) / (2\pi)$ with n^μ being chosen as the fluid velocity u^μ in thermal equilibrium, $\mathcal{J}_+^\mu(p, X)$ and $\mathcal{J}_-^\mu(p, X)$ are the Wigner functions for the right and left-handed fermions, respectively.

Inserting the expression of $\mathcal{J}_\pm^\mu(p, X)$ into Eq. (1) and assuming the chemical potential for left and right handed fermions are identical $\mu_R = \mu_L \equiv \mu$, we can further decompose $\mathcal{S}^\mu(\mathbf{p})$ as [111],

$$\mathcal{S}^\mu(\mathbf{p}) = \mathcal{S}_{\text{thermal}}^\mu(\mathbf{p}) + \mathcal{S}_{\text{shear}}^\mu(\mathbf{p}) + \mathcal{S}_{\text{acc}T}^\mu(\mathbf{p}) + \mathcal{S}_{\text{chemical}}^\mu(\mathbf{p}) + \mathcal{S}_{\text{EB}}^\mu(\mathbf{p}), \quad (3)$$

where

$$\begin{aligned} \mathcal{S}_{\text{thermal}}^\mu(\mathbf{p}) &= \int d\Sigma^\sigma F_\sigma \epsilon^{\mu\nu\alpha\beta} p_\nu \partial_\alpha \frac{u_\beta}{T}, \\ \mathcal{S}_{\text{shear}}^\mu(\mathbf{p}) &= \int d\Sigma^\sigma F_\sigma \frac{\epsilon^{\mu\nu\alpha\beta} p_\nu}{(u \cdot p) T} \{p^\rho (\partial_\rho u_\alpha + \partial_\alpha u_\rho - u_\rho D u_\alpha) u_\beta\} \\ \mathcal{S}_{\text{acc}T}^\mu(\mathbf{p}) &= - \int d\Sigma^\sigma F_\sigma \frac{1}{T} \epsilon^{\mu\nu\alpha\beta} p_\nu u_\alpha (D u_\beta - \frac{1}{T} \partial_\beta T), \\ \mathcal{S}_{\text{chemical}}^\mu(\mathbf{p}) &= 2 \int d\Sigma^\sigma F_\sigma \frac{1}{(u \cdot p)} \epsilon^{\mu\nu\alpha\beta} p_\alpha u_\beta \partial_\nu \frac{\mu}{T}, \\ \mathcal{S}_{\text{EB}}^\mu(\mathbf{p}) &= 2 \int d\Sigma^\sigma F_\sigma \left[\frac{1}{(u \cdot p) T} \epsilon^{\mu\nu\alpha\beta} p_\alpha u_\beta E_\nu + \frac{B^\mu}{T} \right], \end{aligned} \quad (4)$$

and,

$$F^\mu = \frac{\hbar}{8m_\Lambda N} p^\mu f_V^{(0)} (1 - f_V^{(0)}), \quad N = \int d\Sigma^\mu p_\mu f_V^{(0)}, \quad (5)$$

Here, T is the temperature and $f_V^{(0)}$ is the Fermi-Dirac distribution function. The subscripts, *thermal*, *shear*, *accT*, *chemical* and *EB*, stand for the terms related to thermal vorticity, shear viscous tensor, the fluid acceleration minus gradient of temperature ($D u_\beta - \frac{1}{T} \partial_\beta T$), the gradient of μ/T , and electromagnetic fields, respectively. The E^μ and B^μ are given by, $E^\mu = F^{\mu\nu} u_\nu$ and $B^\mu = \frac{1}{2} \epsilon^{\mu\nu\alpha\beta} u_\nu F_{\alpha\beta}$. Note that Ref. [111] has roughly extended the case for massless fermions [88] to the one for massive fermions. For the related decomposition as Eq. (4) for massive fermions, one may refer to Refs. [33, 106–110].

Helicity polarization is defined as [116, 117],

$$S^h = \hat{\mathbf{p}} \cdot \mathcal{S}(\mathbf{p}) = \hat{p}^x \mathcal{S}^x + \hat{p}^y \mathcal{S}^y + \hat{p}^z \mathcal{S}^z, \quad (6)$$

where $\hat{\mathbf{p}} \equiv \mathbf{p}/|\mathbf{p}|$. Inserting Eq. (4) into Eq. (6), we obtain

$$\begin{aligned}
S_{\text{thermal}}^h(\mathbf{p}) &= \int d\Sigma^\sigma F_\sigma p_0 \epsilon^{0ijk} \hat{p}_i \nabla_j \left(\frac{u_k}{T} \right), \\
S_{\text{shear}}^h(\mathbf{p}) &= - \int d\Sigma^\sigma F_\sigma \frac{\epsilon^{0ijk} \hat{p}^i p_0}{(u \cdot p) T} \{ p^\sigma (\partial_\sigma u_j + \partial_j u_\sigma - u_\sigma D u_j) u_k \}, \\
S_{\text{accT}}^h(\mathbf{p}) &= \int d\Sigma^\sigma F_\sigma \frac{1}{T} \epsilon^{0ijk} \hat{p}^i p_0 u_j (D u_k - \frac{1}{T} \partial_k T), \\
S_{\text{chemical}}^h(\mathbf{p}) &= -2 \int d\Sigma^\sigma F_\sigma \frac{1}{(u \cdot p)} p_0 \epsilon^{0ijk} \hat{p}_i \left[\nabla_j \left(\frac{\mu}{T} \right) \right] u_k, \\
S_{\text{EB}}^h(\mathbf{p}) &= 2 \int d\Sigma^\sigma F_\sigma \left[\frac{1}{(u \cdot p) T} \epsilon^{0ijk} \hat{p}^i p_0 E_j u_k + \frac{\hat{p}^i B^i}{T} \right], \tag{7}
\end{aligned}$$

where we implicitly impose the on-shell condition $p_0 = \sqrt{|\mathbf{p}|^2 + m^2}$ with m being the fermionic mass in the end. We emphasize that only the spatial components of thermal vorticity contribute to the helicity polarization. The measurement of the helicity polarization can provide the information of the spatial thermal vorticity, which could present a fine structure of thermal vorticity.

Now we review the symmetric properties for $S_{\text{thermal}}^h(\mathbf{p})$ in hydrodynamical models. For simplicity, we consider $S_{\text{thermal}}^h(\mathbf{p})$ in an ideal fluid and eventually implement our result in a Bjorken flow. More detailed analyses based on symmetries are shown in Refs. [28, 116, 117].

In an ideal fluid, the temperature vorticity,

$$\Omega_T^{\mu\nu} = \partial^\mu (T u^\nu) - \partial^\nu (T u^\mu), \tag{8}$$

is conserved along the velocity, i.e. $\Omega_T^{\mu\nu} u_\nu = 0$ [35, 129, 130] and satisfies the relativistic Kelvin circulation theorem [131–134]. As a consequence, if $\Omega_T^{\mu\nu}$ is zero at initial time, it will always be vanishing during the evolution of this ideal fluid. Then, by using this condition, we can express the $(\partial_\mu u_\nu - \partial_\nu u_\mu)$ as,

$$(\partial_\mu u_\nu - \partial_\nu u_\mu) = -\frac{1}{T} (u_\nu \partial_\mu - u_\mu \partial_\nu) T. \tag{9}$$

Using Eq. (9), we simplify $\mathcal{S}_{\text{thermal}}^\mu(\mathbf{p})$ in Eq. (4),

$$\mathcal{S}_{\text{thermal}}^\mu(\mathbf{p}) = \frac{2}{T^2} \int d\Sigma^\sigma F_\sigma \epsilon^{\mu\nu\alpha\beta} p_\nu (u_\alpha \partial_\beta T). \tag{10}$$

To compute the $\mathcal{S}_{\text{thermal}}^\mu(\mathbf{p})$ in hydrodynamics at the freeze-out hyper-surface, we can assume that the distribution function $f_V^{(0)}$ is approximately at the equilibrium. Then, we can use the relation $\frac{\partial}{\partial p^\sigma} f_V^{(0)} = -\frac{u_\sigma}{T} f_V^{(0)} (1 - f_V^{(0)})$ to remove the fluid velocity and obtain

$$\mathcal{S}_{\text{thermal}}^\mu(\mathbf{p}) = -\frac{1}{4m_\Lambda N} \int d\Sigma_\alpha p^\alpha \epsilon^{\mu\nu\rho\sigma} p_\nu \frac{1}{T} (\partial_\sigma T) \frac{\partial f_V^{(0)}}{\partial p^\rho}, \quad (11)$$

Integrating by parts, we get

$$\begin{aligned} \mathcal{S}_{\text{thermal}}^\mu(\mathbf{p}) &= -\frac{1}{4m_\Lambda N} \epsilon^{\mu\nu\rho\sigma} p_\nu \frac{\partial}{\partial p^\rho} \left[\int d\Sigma_\alpha p^\alpha \frac{1}{T} (\partial_\sigma T) f_V^{(0)} \right] \\ &\quad + \frac{1}{4m_\Lambda N} \epsilon^{\mu\nu\rho\sigma} p_\nu \int d\Sigma_\rho \frac{\partial_\sigma T}{T} f_V^{(0)}. \end{aligned} \quad (12)$$

As argued in Ref. [28, 117], the temperature may be constant at the freeze-out hyper-surface and the direction of $\partial^\mu T$ is approximately parallel to normal vector of hyper-surface Σ^μ . The second term in above equation may therefore vanish at the freeze out hyper surface. Here, we emphasize that in the later hydrodynamic simulations, we did not follow this approximation.

In an ideal fluid with longitudinal boost invariant, the temperature only depends on the proper time $\tau = \sqrt{t^2 - z^2}$ and $\epsilon^{\mu\nu\rho\sigma} (\partial_\sigma T) = \epsilon^{\mu\nu\rho 0} \cosh \eta \frac{dT}{d\tau} - \epsilon^{\mu\nu\rho 3} \sinh \eta \frac{dT}{d\tau}$, where η is spatial rapidity. The spin vector $\mathcal{S}_{\text{thermal}}^\mu(\mathbf{p})$ in Eq. (12) is reduced to [117]

$$\mathcal{S}_{\text{thermal}}^\mu(\mathbf{p}) = -\frac{1}{4m_\Lambda N} p_\nu \frac{\partial}{\partial p^\rho} \left[\int d\Sigma_\alpha p^\alpha f_V^{(0)} (\epsilon^{\mu\nu\rho 0} \cosh \eta - \epsilon^{\mu\nu\rho 3} \sinh \eta) \frac{1}{T} \frac{dT}{d\tau} \right]. \quad (13)$$

Note that only the second term in Eq. (13) contributes to helicity polarization $\mathcal{S}_{\text{thermal}}^h$. At small rapidity Y region, we can approximate that the space-time rapidity is equal to the momentum rapidity, i.e. $\eta \simeq Y$. After taking the Fourier transformation to the azimuthal distribution at the freezeout hypersurface,

$$\int d\Sigma_\lambda p^\lambda f_V^{(0)} = \frac{dN}{2\pi E_p p_T dp_T dY} \left[1 + \sum_{n=1}^{\infty} 2v_n(p_T, Y) \cos n\phi \right], \quad (14)$$

the polarization vector $\mathcal{S}_{\text{thermal}}^\mu(\mathbf{p})$ and helicity polarization $S^h(\mathbf{p})$ read [28, 117],

$$\begin{aligned} \mathcal{S}_{\text{thermal}}^z &= -\frac{1}{4m_\Lambda N} \frac{1}{T} \frac{dT}{d\tau} \Big|_\Sigma \partial_\phi \int d\Sigma_\alpha p^\alpha f_V^{(0)} \cosh \eta \\ &\approx \frac{1}{4m_\Lambda} \frac{1}{T} \frac{dT}{d\tau} \Big|_\Sigma \left[\sum_{n=1}^{\infty} 2nv_n(p_T, Y) \sin n\phi \right], \end{aligned} \quad (15)$$

$$\begin{aligned} \mathcal{S}_{\text{thermal}}^h &= -\frac{1}{4m_\Lambda N} \frac{1}{T} \frac{dT}{d\tau} \Big|_\Sigma \partial_\phi \int d\Sigma_\alpha p^\alpha f_V^{(0)} \sinh \eta \\ &\approx \frac{Y}{4m_\Lambda} \frac{1}{T} \frac{dT}{d\tau} \Big|_\Sigma \left[\sum_{n=1}^{\infty} 2nv_n(p_T, Y) \sin n\phi \right]. \end{aligned} \quad (16)$$

From Eqs. (15) and (16), it implies that in the small rapidity region $Y \sim 0$ [28, 117],

$$S_{\text{thermal}}^h(Y, \phi_p) \approx Y \mathcal{S}_{\text{thermal}}^z(Y, \phi_p). \quad (17)$$

Meanwhile, for a given rapidity, the elliptical flow coefficient v_2 is larger than other coefficients v_n . Therefore, Eq. (15) can also be written as in small rapidity region $Y \sim 0$,

$$\mathcal{S}_{\text{thermal}}^z \approx \frac{1}{m_\Lambda} \frac{1}{T} \left. \frac{dT}{d\tau} \right|_\Sigma v_2(p_T, 0) \sin 2\phi. \quad (18)$$

In hydrodynamic simulations, the system is beyond the ideal Bjorken flow, we therefore expect that the condition (17) is approximately satisfied. We will revisit Eq. (17) after the rapidity integration in Sec. III.

Meanwhile, the system should have the space reversal symmetry [28, 116], i.e. $\mathbf{S}(\mathbf{p}) = \mathbf{S}(-\mathbf{p})$, or

$$\mathcal{S}(Y, \phi_p) = \mathcal{S}(-Y, \phi_p + \pi), \quad (19)$$

and from Eq. (6) we can obtain the following relation,

$$S^h(Y, \phi_p) = -S^h(-Y, \phi_p + \pi). \quad (20)$$

Note that, Eq. (20) should be satisfied for each part in Eq. (7). We will test it in the later hydrodynamic simulations.

At last, let us discuss the frame dependence of helicity polarization. All the quantities mentioned above are chosen in the laboratory frame. In experiments, the polarization of Λ and $\bar{\Lambda}$ hyperons are measured in their own rest frames. Since the momentum in the rest frame of hyperons $p'^\mu = (m_\Lambda, 0)$ is related to the momentum $p^\mu = (E_\Lambda, \mathbf{p})$ in the laboratory frame by Lorentz transformation, i.e. $p'^\mu = \Lambda^\mu_\nu p^\nu$, we obtain the polarization vector \mathcal{S}'^μ in the rest frame of hyperons,

$$\mathcal{S}'^\mu = \left(0, \mathcal{S} - \frac{(\mathbf{p} \cdot \mathcal{S}) \mathbf{p}}{E_\Lambda(E_\Lambda + m_\Lambda)} \right). \quad (21)$$

Similar to the definition in Eq. (6), one can also define the helicity polarization as $\hat{\mathbf{p}} \cdot \mathcal{S}'$, which is connected to our helicity polarization S^h by,

$$\hat{\mathbf{p}} \cdot \mathcal{S}' = \frac{m_\Lambda}{E_\Lambda} \hat{\mathbf{p}} \cdot \mathcal{S} = \frac{m_\Lambda}{E_\Lambda} S^h. \quad (22)$$

Therefore, it is straightforward to transform our simulation results to $\hat{\mathbf{p}} \cdot \mathcal{S}'$ [28, 116].

Before end this section, we emphasize that in general the axial chemical potential $\mu_A = \mu_R - \mu_L$ can also contribute to the $\mathcal{S}^\mu(\mathbf{p})$ and leads to the extra helicity polarization, which could be a possible signal of the parity violation [116]. Since we have already assumed that $\mu_A = 0$ in Eqs. (4), there are no such corrections in our case. One can also see Refs. [50, 114, 116] for other corrections for $\mathcal{S}^\mu(\mathbf{p})$.

III. NUMERICAL RESULTS FROM HYDRODYNAMICS APPROACH

In this section, we study the the azimuthal angle ϕ_p and the momentum rapidity Y dependence of helicity polarization S^h in the hydrodynamic model and compare our results with those in an ideal Bjorken flow shown in Sec. II.

A. Setup

We implement the open source (3+1) dimensional viscous hydrodynamic package CLVisc [135] with AMPT initial conditions [34, 35, 136] at 20%–50% centrality to study the helicity polarization in $\sqrt{s_{NN}} = 200$ GeV Au+Au collisions. Similar to our previous work in Ref. [111], we choose $\eta/s = 1/(4\pi)$, the freeze-out temperature $T = 157$ MeV and “*s95p-pce*” [137] as equation of state to generate the information of the freeze-out hyper-surface Σ^μ .

By using the Eq. (6), we define the azimuthal angle ϕ_p dependent helicity polarization as,

$$P_H(\phi_p) = \frac{2}{\mathcal{M}(+\Delta Y, -\Delta Y)} \int_{-\Delta Y}^{+\Delta Y} dY \int_{p_T^{min}}^{p_T^{max}} dp_T p_T [N S^h(\mathbf{p})], \quad (23)$$

where N is defined in Eq. (5) and the normalization factor is given by,

$$\mathcal{M}(Y_{max}, Y_{min}) = \int_{Y_{min}}^{Y_{max}} dY \int_{p_T^{min}}^{p_T^{max}} dp_T p_T N, \quad (24)$$

Note that, one can also define the averaged helicity polarization as, $P_H(\phi_p) = \frac{1}{\Delta Y} \int_{-\Delta Y}^{+\Delta Y} dY \frac{1}{\Delta p_T} \int_{p_T^{min}}^{p_T^{max}} dp_T S^h(\mathbf{p})$. The definition (23) used in the current work is close to the local and global polarization measured in the experiments. where the $p_T = \sqrt{p_x^2 + p_y^2}$ is the transverse momentum and $\Delta p_T \equiv p_T^{max} - p_T^{min}$. We have chosen $p_T^{max} = 3$ GeV and $p_T^{min} = 0$ GeV in our calculation and concentrate on the mid-rapidity $[-1, +1]$, i.e. $\Delta Y = 1$.

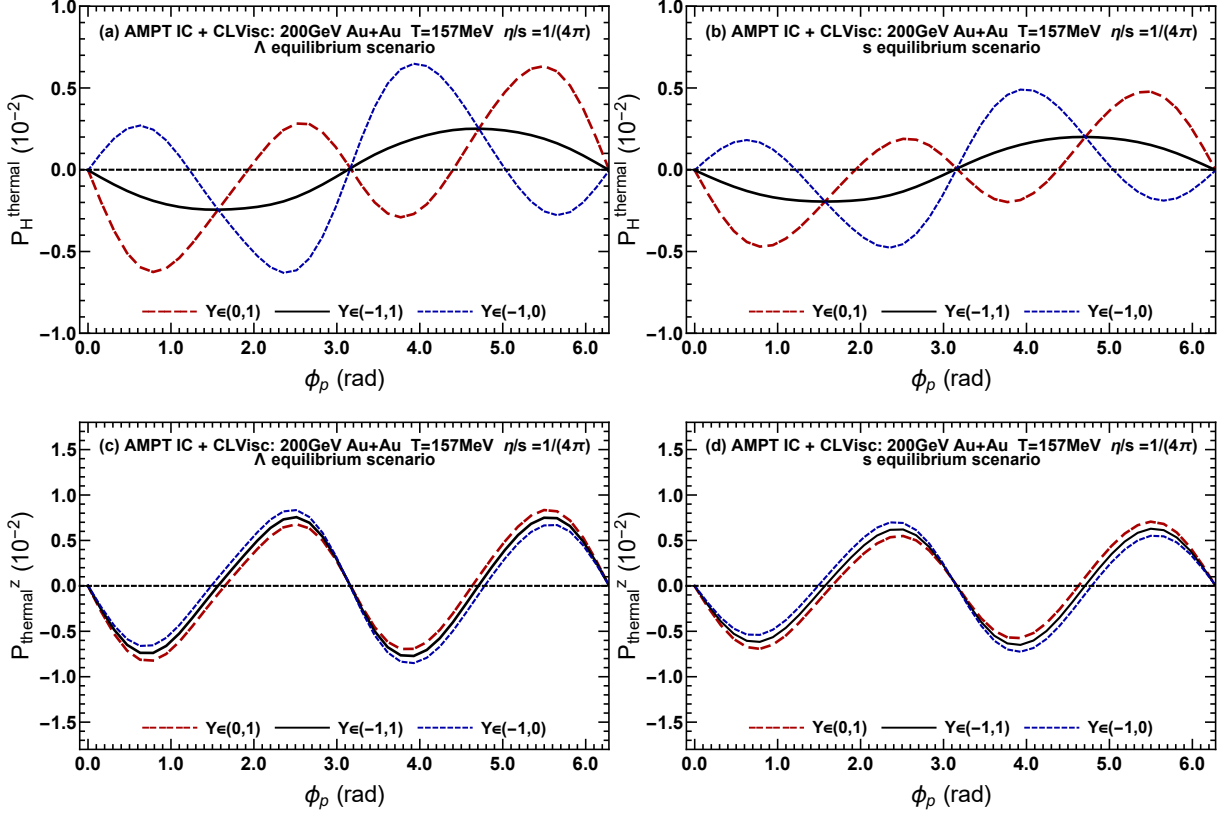


Figure 1: The helicity polarization P_H^{thermal} and spin polarization along the beam direction P_{thermal}^z contributed by thermal vorticity as a function of ϕ_p in upper and lower plane, respectively. The results for Λ and s equilibrium scenario are shown in the left and right handed side, respectively. Black solid, red dash-dotted and blue dashed lines stand for helicity polarization P_H^{thermal} , $P_H^{+\text{thermal}}$, $P_H^{-\text{thermal}}$ or spin polarization P_{thermal}^z , P_{thermal}^{+z} , P_{thermal}^{-z} in the upper and lower plane, respectively.

In order to test the theoretical result in Eq. (16), we also introduce the $P_H^+(\phi_p)$ and $P_H^-(\phi_p)$,

$$\begin{aligned}
 P_H^+(\phi_p) &= \frac{2}{\mathcal{M}(+\Delta Y, 0)} \int_0^{+\Delta Y} dY \int_{p_T^{\min}}^{p_T^{\max}} dp_T p_T [N S^h(\mathbf{p})], \\
 P_H^-(\phi_p) &= \frac{2}{\mathcal{M}(0, -\Delta Y)} \int_{-\Delta Y}^0 dY \int_{p_T^{\min}}^{p_T^{\max}} dp_T p_T [N S^h(\mathbf{p})].
 \end{aligned} \tag{25}$$

According to Eq. (7), we can also decompose P_H , P_H^+ , P_H^- into 5 terms. Since the electromagnetic field decays rapidly in the relativistic heavy ion collision [138, 139], we ignore the helicity polarization contributed by EB term. Since the gradient of chemical potential μ is negligible for the $\sqrt{s_{NN}} = 200$ GeV Au+Au high-energy collisions and the information

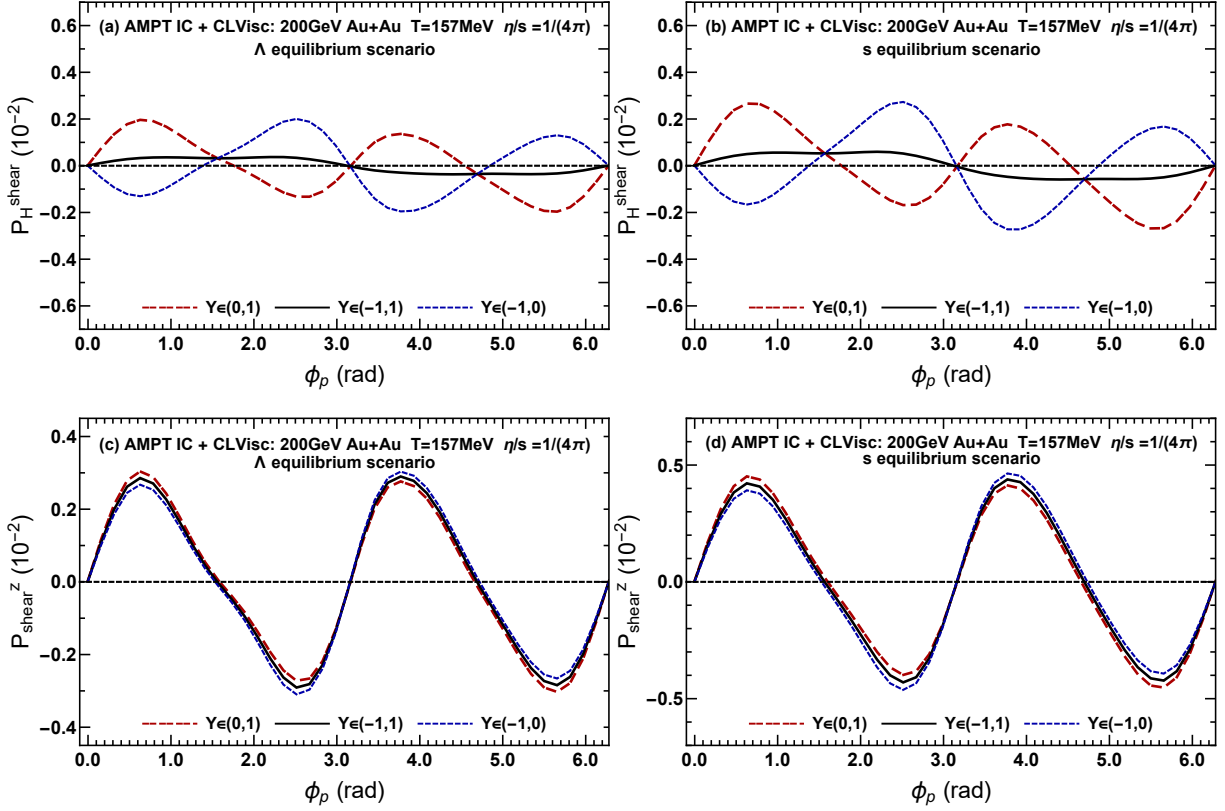


Figure 2: The helicity polarization P_H^{shear} and local spin polarization along the beam direction P_{shear}^z induced by shear viscous tensor as a function of ϕ_p for Λ and s equilibrium scenarios. We use the same setup and color assignments as those in Fig. 1.

of chemical potential lacks in EoS "*s95pce*", we also neglect the helicity polarization related to chemical potential. Therefore, we only consider the following parts,

$$\begin{aligned}
 P_H^{\text{total}} &= P_H^{\text{thermal}} + P_H^{\text{shear}} + P_H^{\text{accT}}, \\
 P_H^{+\text{total}} &= P_H^{+\text{thermal}} + P_H^{+\text{shear}} + P_H^{+\text{accT}}, \\
 P_H^{-\text{total}} &= P_H^{-\text{thermal}} + P_H^{-\text{shear}} + P_H^{-\text{accT}},
 \end{aligned} \tag{26}$$

where the upper indices stand for the helicity polarization contributed by the thermal vorticity, shear viscous tensor and fluid acceleration, respectively.

Similarly, we also introduce the local spin polarization at different momentum rapidity

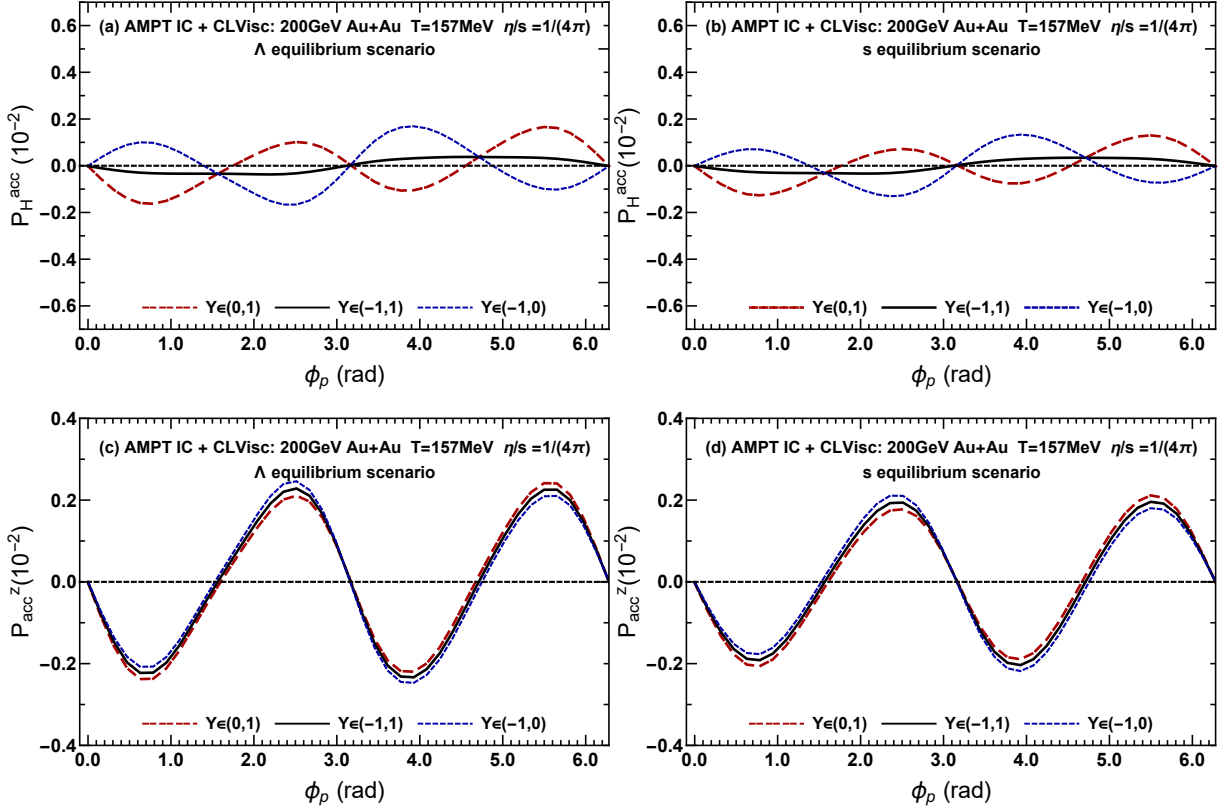


Figure 3: The helicity polarization P_H^{acc} and local spin polarization along the beam direction P_{acc}^z induced by fluid acceleration as a function of ϕ_p for Λ and s equilibrium scenarios. We use the same setup and color assignments as those in Fig. 1.

range,

$$\begin{aligned}
P^i(\phi_p) &= \frac{2}{\mathcal{M}(+\Delta Y, -\Delta Y)} \int_{-\Delta Y}^{+\Delta Y} dY \int_{p_T^{\min}}^{p_T^{\max}} dp_T p_T [N \mathcal{S}^i(\mathbf{p})], \\
P^{i+}(\phi_p) &= \frac{2}{\mathcal{M}(+\Delta Y, 0)} \int_0^{+\Delta Y} dY \int_{p_T^{\min}}^{p_T^{\max}} dp_T p_T [N \mathcal{S}^i(\mathbf{p})], \\
P^{i-}(\phi_p) &= \frac{2}{\mathcal{M}(0, -\Delta Y)} \int_{-\Delta Y}^0 dY \int_{p_T^{\min}}^{p_T^{\max}} dp_T p_T [N \mathcal{S}^i(\mathbf{p})].
\end{aligned} \tag{27}$$

where the \mathcal{S}^i is defined in Eq. (1) and $i = x, y, z$ stands for the polarization along the in-plane, out-of-plane, and beam directions, respectively. We further decompose the polarization along the beam direction P^z , P^{z+} , P^{z-} into 3 term.

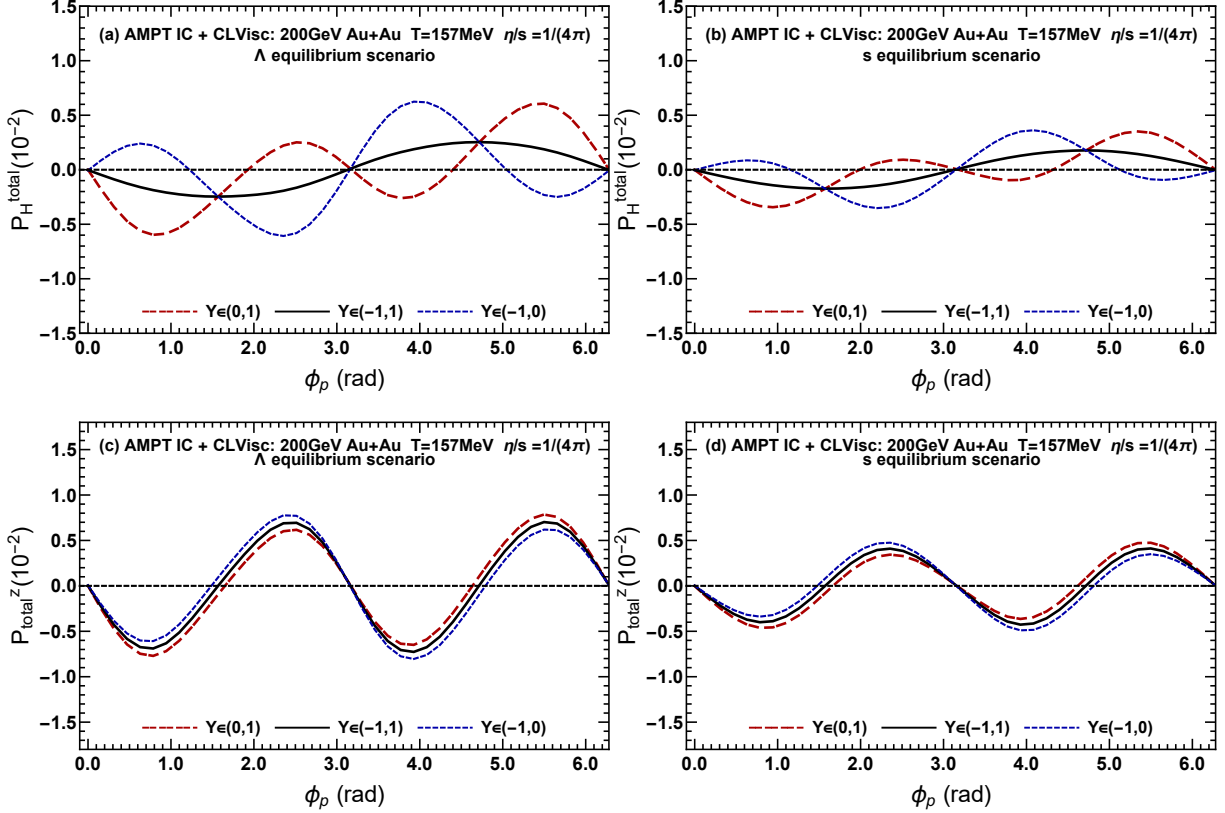


Figure 4: The total helicity polarization P_H^{total} and local spin polarization along the beam direction P^z_{total} as a function of ϕ_p for Λ and s equilibrium scenarios. We use the same setup and color assignments as those in Fig. 1.

$$\begin{aligned}
P^z &= P^z_{\text{thermal}} + P^z_{\text{shear}} + P^z_{\text{acc}}, \\
P^{z+} &= P^{z+}_{\text{thermal}} + P^{z+}_{\text{shear}} + P^{z+}_{\text{acc}}, \\
P^{z-} &= P^{z-}_{\text{thermal}} + P^{z-}_{\text{shear}} + P^{z-}_{\text{acc}}.
\end{aligned} \tag{28}$$

As proposed in Ref. [109] and also used in our previous work [111], we consider two different scenarios, named Λ and s *equilibrium scenarios*. In the Λ equilibrium scenario, we assume that the Λ hyperons are near the local equilibrium after they are produced at chemical freezeout. We then use the information in the freeze-out hypersurface to describe the thermodynamic state of the Λ hyperons. In the s equilibrium scenario, according to the parton models, we assume that the spin polarization of Λ is mainly contributed by the s quark, and the spin polarization of the s quark is close to the spin polarization of Λ

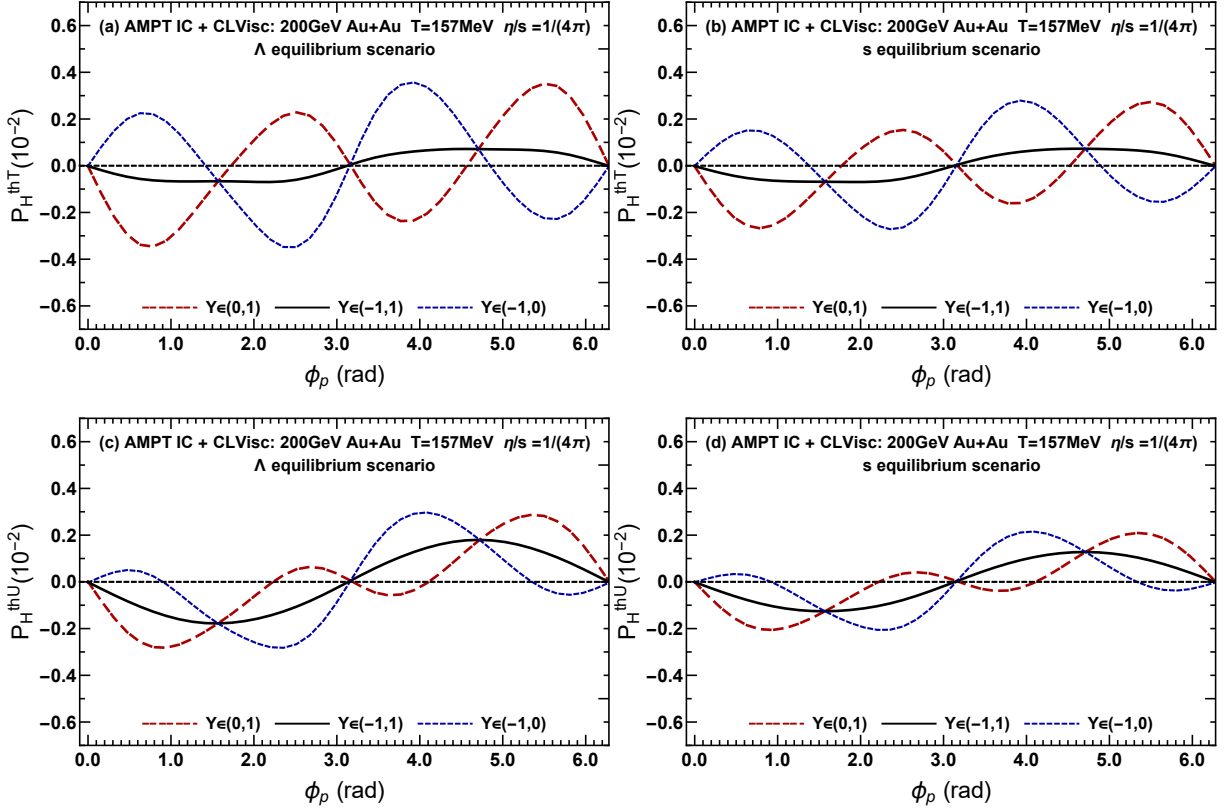


Figure 5: The helicity polarization P_H^{thT} (up) and P_H^{thU} (down) separated by P_H^{thermal} , as a function of ϕ_p for Λ and s equilibrium scenarios. We use the same setup and color assignments as those in Fig. 1.

hyperons. In these two scenarios, the mass of particles are chosen as $m = m_\Lambda = 1.116$ GeV and $m = m_s = 0.3$ GeV (constituent quark mass) and we use the same information of the freezeout hyper-surface.

B. Numerical result

We present the numerical results for helicity polarization P_H and the polarization along the beam direction P^z in Eq. (25) and Eq. (27) as functions of azimuthal angle ϕ_p and momentum rapidity Y at $\sqrt{s_{NN}} = 200$ GeV Au-Au collisions in 20 – 50% centrality. Note that both P_H and P^z are calculated in laboratory frame in our numerical simulations.

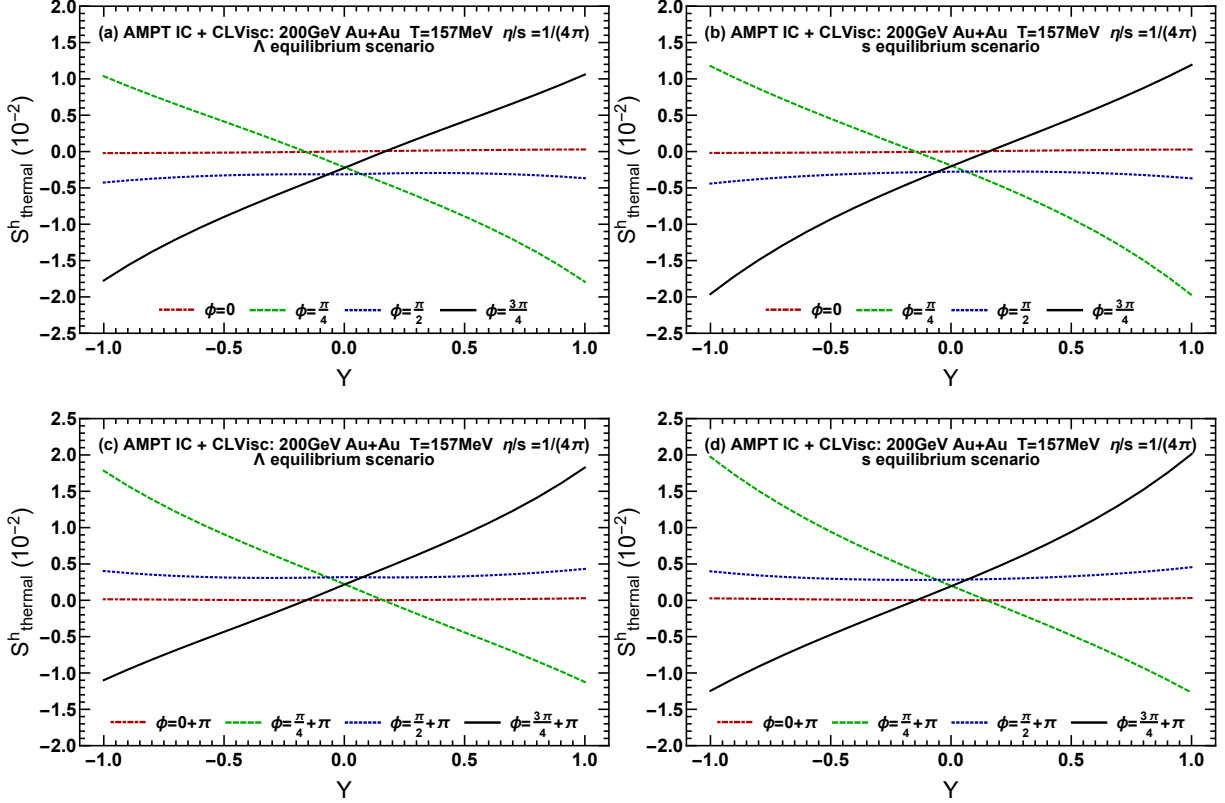


Figure 6: The helicity polarization scalar S_{thermal}^h induced by thermal vorticity as a function of momentum rapidity Y with different azimuthal angle ϕ_p in Λ and s equilibrium scenarios. We use the same setup as those in Fig. 1. Colors stand for the different angle ϕ_p .

1. Azimuthal angle dependence

In Fig. 1, we plot the azimuthal angle dependent helicity polarization and spin polarization induced by thermal vorticity with the three different integral areas. To understand the Fig. 1, let us estimate the P_H^{thermal} , $P_H^{\pm\text{thermal}}$ by using Eq. (16). According to the definitions of $P_H^{\pm\text{thermal}}$, P_{thermal}^z in Eqs.(25, 27), we find that in a Bjorken flow and $Y \simeq 0$ limit,

$$P_H^{\pm,\text{thermal}} \simeq \pm(\Delta Y)^2 P_{\text{thermal}}^{z,\pm}. \quad (29)$$

For our case, $\Delta Y = 1$, we expect that $\text{sign}(P_H^{\pm\text{thermal}}) = \pm\text{sign}(P_{\text{thermal}}^{z,\pm})$, $P_H^{\text{thermal}} = -P_H^{-\text{thermal}}$, and $P_H^{\text{thermal}} \simeq 0$ for arbitrary ϕ_p . We observe that although the relation for the signs of $P_H^{\pm\text{thermal}}$ and $P_{\text{thermal}}^{z,\pm}$ are approximately close to our expectation, the difference between P_H^{thermal} and $-P_H^{-\text{thermal}}$ is not negligible for both the Λ and s equilibrium scenarios. The reason is that we simulate the dissipative fluids beyond the assumption of ideal Bjorken

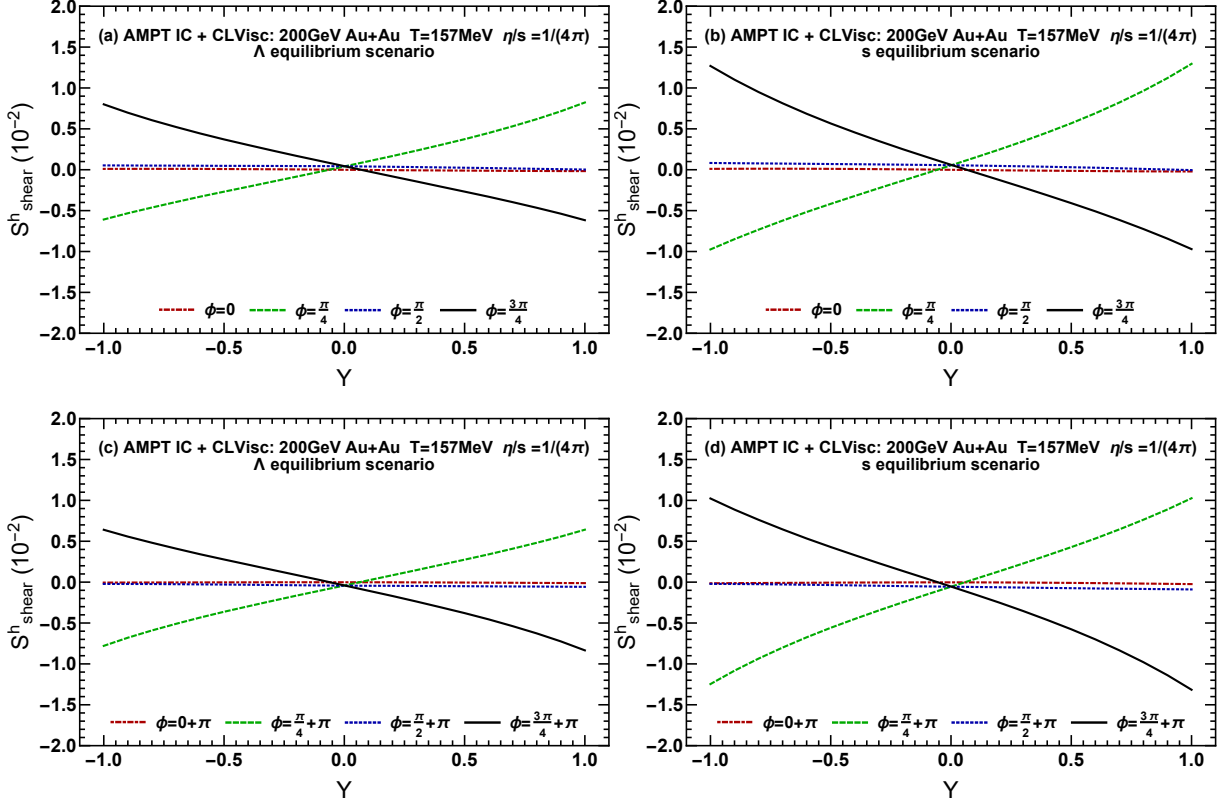


Figure 7: The helicity polarization scalar S_{shear}^h induced by shear viscous tensor as a function of momentum rapidity Y for Λ and s equilibrium scenarios. We use the same setup as those in Fig. 1. Colors stand for the different angle ϕ_p .

flows used in Eq. (16). Interestingly, we observe the similar pattern for helicity polarization P_H and spin polarization P^z induced by shear viscous tensor and fluid acceleration in Figs. 2, 3 and 4.

Other important observation in Figs. 1,2,3,4 is that the period of $P_H^{\text{thermal}}, P_H^{\text{shear}}, P_H^{\text{accT}}, P_H^{\text{total}}$ as a function of ϕ_p are approximately 2π , which are different with P^i . Our general discussion is as follows. According to definition of S^h in Eq. (6), the non-vanishing P_H mainly comes from the additional contributions from \mathcal{S}^x and \mathcal{S}^y . Although the period of $\mathcal{S}(\phi_p)$ is π shown in Eq. (19), the period of $\int_{-\Delta Y}^{+\Delta Y} dY (\hat{p}^x \mathcal{S}^x + \hat{p}^y \mathcal{S}^y)$ should be 2π instead of π since $p^x \propto \cos \phi_p$ and $p^y \propto \sin \phi_p$. To clarify this, we integrate over the rapidity and p_T in Eq. (16) and obtain that P_H in a Bjorken flow,

$$P_H \propto (\Delta Y)^3 \left. \frac{dT}{d\tau} \right|_{\Sigma} \int dp_T p_T \left. \frac{\partial v_1}{\partial Y} \right|_{Y \rightarrow 0} \sin \phi_p, \quad (30)$$

which also implies that the period of P_H is approximately 2π instead of π . It is consistent

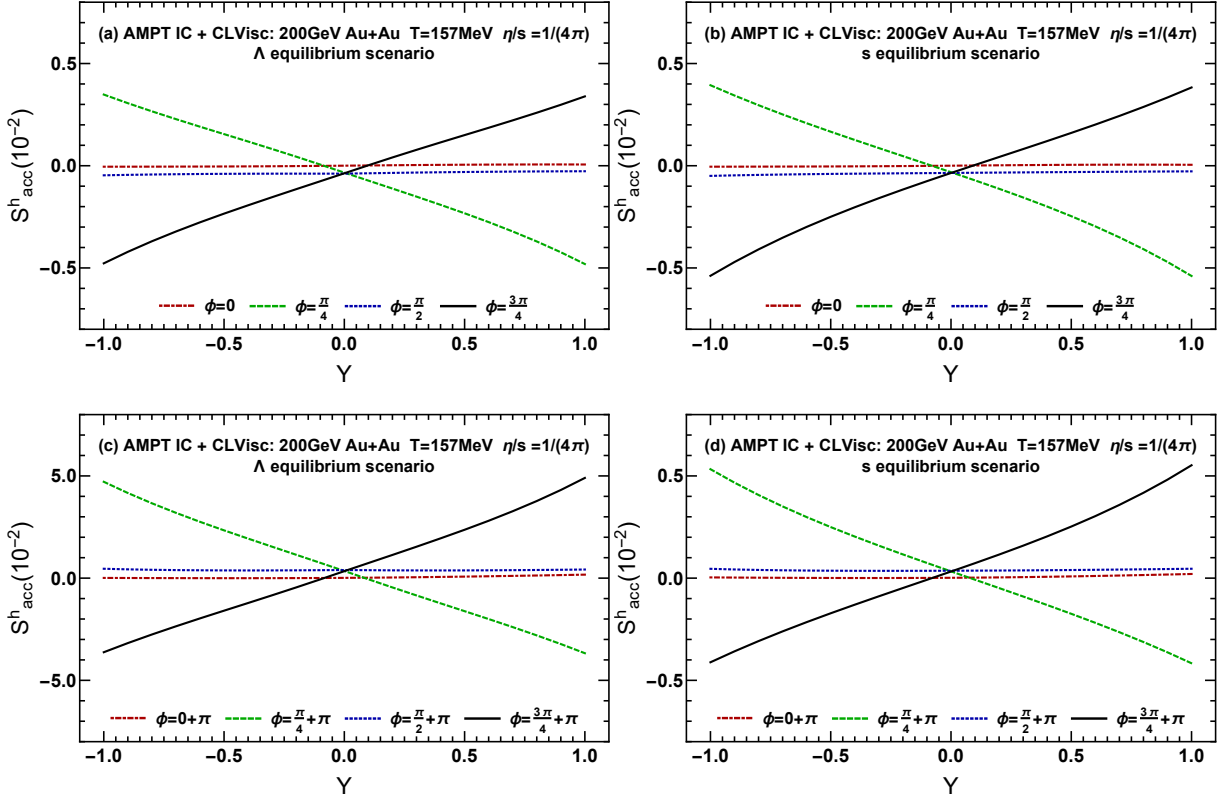


Figure 8: The helicity polarization scalar S^h_{acc} induced by the fluid acceleration as a function of momentum rapidity Y for Λ and s equilibrium scenarios. We use the same setup as those in Fig. 1. Colors stand for the different angle ϕ_p .

with the analysis in $Y = 0$ limit shown in Ref. [116].

Remarkably, the future measurement of helicity polarization may help us to distinguish the thermal-vorticity induced spin polarization with the others in local spin polarization. In Figs. 1, 2, 3, 4, we observe that the shear and fluid acceleration induced helicity polarization $P_H^{\text{shear}}, P_H^{\text{accT}}$ are much smaller than P_H^{thermal} , i.e. $P_H \simeq P_H^{\text{thermal}}$ in both Λ and s quark scenarios of our simulations. Therefore, it may be possible to fix the value of thermal induced local spin polarization $P_{\text{thermal}}^{x,y,z}$ by matching the results from numerical simulations for P_H^{thermal} with the data of P_H from the future experiments.

To understand the above observation, let us take a close look to the expression of S_{shear}^h ,

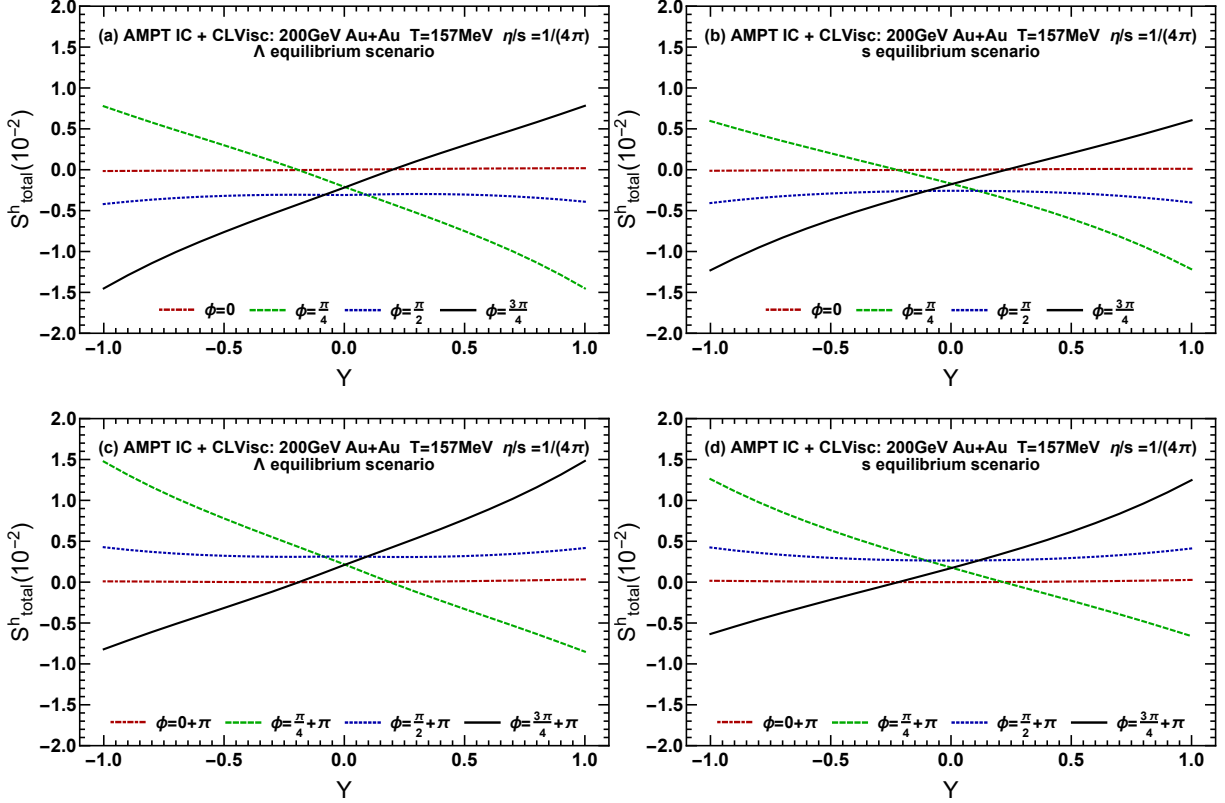


Figure 9: The total helicity polarization scalar S_{total}^h as a function of momentum rapidity Y for Λ and s equilibrium scenario. We use the same setup as those in Fig. 1. Colors stand for the different angle ϕ_p .

S_{accT}^h and S_{thermal}^h in Eqs. (7). We can further decompose S_{thermal}^h as two parts,

$$\begin{aligned}
 S_{\text{thT}}^h(\mathbf{p}) &= \int d\Sigma^\sigma F_\sigma \frac{p_0}{T^2} \hat{\mathbf{p}} \cdot (\mathbf{u} \times \nabla T), \\
 S_{\text{thU}}^h(\mathbf{p}) &= \int d\Sigma^\sigma F_\sigma \frac{p_0}{T} \hat{\mathbf{p}} \cdot \boldsymbol{\omega},
 \end{aligned} \tag{31}$$

where ∇ represents the spatial component of ∂_μ and $\boldsymbol{\omega} = \nabla \times \mathbf{u}$ denotes the fluid vorticity. Note that, S_{shear}^h , S_{accT}^h and S_{thT}^h are proportional to the integration of fluid velocity \mathbf{u} , while S_{thU}^h is proportional to the integration of the space derivative of \mathbf{u} only. From Figs. 2,3 and 5, it seems that these effects proportional to fluid velocity \mathbf{u} are approximately symmetric in the rapidity area $[-1, 0]$ and $[0, +1]$. The difference of S_{thU}^h in rapidity area $[-1, 0]$ and $[0, +1]$ are significant. That incomplete cancellation of S_{thU}^h in two rapidity area causes the thermal induced helicity polarization dominates in P_H .

It is also clear to see $P_H^{\text{thU}} \gtrsim 2P_H^{\text{thT}}$ as shown in Fig. 5 (in central rapidity $[-1, 1]$). We

would like to comment that in low-energy collisions the contributions from fluid vorticity are expected to be significant enhanced due to the nuclear-stopping effect [140, 141], while the gradient of temperature may reduce. In such a case, we expect that in low-energy collisions P_H^{total} is mostly led by the contribution from fluid vorticity. Accordingly, by measuring P_H^{total} , one may estimate the local magnitude of $|\boldsymbol{\omega}|$ in low energy collisions. We also test these results in different sets of parameters and find that the conclusion holds.

At last, we discuss the results in two different scenarios. We observe that $P_H^{+\text{thermal}}$, $P_H^{-\text{thermal}}$ and P_H^{thermal} are almost the same in two scenarios shown in Fig. 1. Both the expression of S_{thermal}^h or $\mathcal{S}_{\text{thermal}}^\mu$ in Eqs. (4, 7) and the previous numerical simulations in different studies [109, 111] indicate that $\mathcal{S}_{\text{thermal}}^{x,y,z}$ in the lab frame is insensitive to the particles' mass expect for the over-all factor m_Λ in the denominator. Our findings are consistent with the previous results. For the similar reason, the difference of $P_H^{+\text{accT}}$, $P_H^{-\text{accT}}$ and P_H^{accT} in two scenarios is also small. However, the shear induced local spin polarization are very sensitive to the mass [109, 111] due to the extra $(u \cdot p) \sim m$ in the denominator inside the integral shown in Eq. (4). That is why we observe a significant enhancement of P_H^{shear} in s quark scenario in Fig. 2.

2. Momentum rapidity dependence

In the Figs. 6, 7, 8, 9, we plot the $S_{\text{thermal}}^h, S_{\text{shear}}^h, S_{\text{accT}}^h, S_{\text{total}}^h$ as a function of momentum rapidity Y at different angle $\phi_p = 0, \pi/4, \pi/2, 3\pi/4, \pi, 5\pi/4, 3\pi/2, 7\pi/2$ for the Λ and the s equilibrium scenarios and observe the space reversal symmetry. According to the space reversal symmetry in Eq.(20), it is clearly shown in these figures that $S^h(Y, \phi_p) = -S^h(-Y, \phi_p + \pi)$.

Interestingly, we find at $\phi_p = \pi/2, 3\pi/2$, only $S_{\text{thermal}}^h(\phi_p = \pi/2)$ is nonzero, while S_{shear}^h and S_{accT}^h are almost vanishing. It is straightforward to explain this behavior. When $\phi_p = \pi/2, 3\pi/2$, since $\hat{p}^x = 0$ and $\mathcal{S}^z \simeq 0$ from both numerical simulations [109, 111] and experimental data [26, 27], $S^h(\phi_p = \pi/2) \simeq \hat{p}^y \mathcal{S}^y(\phi_p = \pi/2)$ with the help of Eq. (6), while the $\mathcal{S}_{\text{shear}}^y$ and $\mathcal{S}_{\text{accT}}^y$ are found to be close to zero at $\phi_p = \pi/2$ [111]. Eventually, the nonzero $\mathcal{S}_{\text{thermal}}^y$ gives finite S_{thermal}^h at $\phi_p = \pi/2$. When $\phi_p = 0, \pi$, $\mathcal{S}^{x,z}$ is found to be zero and $\hat{p}^y = 0$, which leads to $S^h = 0$ from Eq. (6). The arguments above explain what we observed in these figures.

Next, we discuss the slopes of S^h at several special angles. At $\phi_p = 0, \pi/2, \pi, 3\pi/2$, \mathcal{S}^z

vanishes, S^h should mainly come from $\mathcal{S}^{x,y}$. Since $\widehat{p}^x, \widehat{p}^y$ are independent on Y and \mathcal{S}^y is almost independent on Y from experimental observations [20, 142, 143], we find slow variation of S^h as a function of Y at $\phi_p = 0, \pi/2, \pi, 3\pi/2$. Since \mathcal{S}^z at other ϕ_p is nonzero and it contributes to the final S^h through $\widehat{p}^z \sim \sin Y$, S^h is very sensitive to Y when $\phi_p \neq 0, \pi/2, \pi, 3\pi/2$.

IV. CONCLUSIONS AND DISCUSSIONS

We have studied the helicity polarization in hydrodynamic approaches. Following our previous work [111], we decompose the helicity polarization S^h introduced in Refs. [116, 117] into several components in local equilibrium, such as helicity polarization induced by thermal vorticity $S_{\text{thermal}}^h(\mathbf{p})$, shear viscous tensor $S_{\text{shear}}^h(\mathbf{p})$, fluid acceleration $S_{\text{accT}}^h(\mathbf{p})$, other terms related to electromagnetic fields $S_{\text{EB}}^h(\mathbf{p})$, and the gradient of the ratio to a vector chemical potential and temperature $S_{\text{chemical}}^h(\mathbf{p})$. For simplicity, we neglect possible contributions from an axial chemical potential. We then obtain the space reversal symmetry of S^h in Eq.(20) and discuss the property of $S_{\text{thermal}}^h(\mathbf{p})$ in the ideal Bjorken flow shown in Eq. (16). We then implement the (3+1) dimensional viscous hydrodynamic package CLVisc with AMPT initial conditions at 20% – 50% centrality of $\sqrt{s_{NN}} = 200$ GeV Au-Au collisions to study helicity polarization. We neglect $S_{\text{EB}}^h(\mathbf{p})$ and $S_{\text{chemical}}^h(\mathbf{p})$ in current studies and analyze the azimuthal angle ϕ_p and the momentum rapidity Y dependence of helicity polarization contributed by $S_{\text{thermal}}^h(\mathbf{p})$, $S_{\text{shear}}^h(\mathbf{p})$ and $S_{\text{accT}}^h(\mathbf{p})$ in Λ and s equilibrium scenarios.

We find that the hydrodynamic simulations are beyond the theoretical expectation in Eq. (16) for the ideal Bjorken flow. Different from the local spin polarization vectors \mathcal{S}^μ , the helicity polarization P_H has a period 2π instead of π . Remarkably, we find the thermal induced helicity polarization P_H^{thermal} dominates total P_H . In particular, the helicity polarization contributed by fluid vorticity, S_{thU}^h , is much larger than the contributions from other components. Similar to local spin polarization, only shear induced helicity polarization has the significant enhancement in the s equilibrium scenario. We also observe the strict space reversal symmetry for S^h expected in Eq. (20).

As a first attempt, our studies provide the baseline for the future investigation on the correlation of helicity polarization induced by the axial chemical potential, which is a possible signal of local parity violation proposed by Ref. [28, 116, 117]. Meanwhile, since we find that

the helicity polarization P_H mainly comes from the thermal induced local spin polarization $\mathcal{S}_{\text{thermal}}^\mu$. In the future measurements of helicity polarization, one might match the numerical simulations of $\mathcal{S}_{\text{thermal}}^\mu$ or P_H^{thermal} with the experimental data of P_H . It may help us to distinguish the $\mathcal{S}_{\text{thermal}}^\mu$ from local spin polarization induced by other effects.

Furthermore, P_H serves as a more direct signal to characterize locally how vortical the quark gluon plasma is and we may extract the magnitude of local fluid vorticity $|\boldsymbol{\omega}|$. In current study, we find that P_H^{thU} is much larger than other components in the helicity polarization. Because the enhancement of fluid vorticity in low-energy collisions due to the nuclear-stopping effect [140, 141], the P_H^{thU} is expected to dominate P_H in low-energy collisions. Therefore, it is tentative to further investigate the helicity polarization in both theory and experiment to extract possibly strongest local fluid vorticity from the beam energy scan.

Acknowledgments

We would like to thank Xiang-yu Wu, Hong-zhong Wu for helpful discussion. S.P. is supported by National Natural Science Foundation of China (NSFC) under Grants No. 1207523 and No. 12135011. J.H. Gao was supported in part by the National Natural Science Foundation of China under Grant Nos. 11890710, 11890713 and 12175123, and the Major Program of Natural Science Foundation of Shandong Province under Grant No. ZR2020ZD30. D.-L. Y. was supported by the Ministry of Science and Technology, Taiwan under Grant No. MOST 110-2112-M-001-070-MY3.

-
- [1] S. J. Barnett, Rev. Mod. Phys. **7**, 129 (1935).
 - [2] Z.-T. Liang and X.-N. Wang, Phys. Lett. **B629**, 20 (2005), nucl-th/0411101.
 - [3] Z.-T. Liang and X.-N. Wang, Phys. Rev. Lett. **94**, 102301 (2005), nucl-th/0410079, [Erratum: Phys. Rev. Lett.96,039901(2006)].
 - [4] STAR, L. Adamczyk *et al.*, Nature **548**, 62 (2017), 1701.06657.
 - [5] F. Becattini and F. Piccinini, Annals Phys. **323**, 2452 (2008), 0710.5694.
 - [6] F. Becattini, F. Piccinini, and J. Rizzo, Phys. Rev. C **77**, 024906 (2008), 0711.1253.

- [7] F. Becattini, V. Chandra, L. Del Zanna, and E. Grossi, *Annals Phys.* **338**, 32 (2013), 1303.3431.
- [8] R.-H. Fang, L.-G. Pang, Q. Wang, and X.-N. Wang, *Phys. Rev.* **C94**, 024904 (2016), 1604.04036.
- [9] I. Karpenko and F. Becattini, *The European Physical Journal C* **77**, 213 (2017).
- [10] Y. Xie, D. Wang, and L. P. Csernai, *Phys. Rev. C* **95**, 031901 (2017).
- [11] H. Li, L.-G. Pang, Q. Wang, and X.-L. Xia, *Phys. Rev. C* **96**, 054908 (2017).
- [12] Y. Sun and C. M. Ko, *Phys. Rev.* **C96**, 024906 (2017), 1706.09467.
- [13] S. Shi, K. Li, and J. Liao, *Physics Letters B* **788**, 409 (2019).
- [14] D.-X. Wei, W.-T. Deng, and X.-G. Huang, *Phys. Rev. C* **99**, 014905 (2019).
- [15] S. Shi, H. Zhang, D. Hou, and J. Liao, (2019), 1910.14010.
- [16] B. Fu, K. Xu, X.-G. Huang, and H. Song, *Phys. Rev. C* **103**, 024903 (2021), 2011.03740.
- [17] S. Ryu, V. Jupic, and C. Shen, (2021), 2106.08125.
- [18] A. Lei, D. Wang, D.-M. Zhou, B.-H. Sa, and L. P. Csernai, *Phys. Rev. C* **104**, 054903 (2021), 2110.13485.
- [19] F. K. for HADES Collaboration, in *talks given at Strangeness Quark Matter 2021, Online, May 17-22,2021 and the 6th International Conference on Chirality, Vorticity and Magnetic Field in HIC, Online, Nov. 1-5,2021*.
- [20] STAR, M. S. Abdallah *et al.*, (2021), 2108.00044.
- [21] Y. B. Ivanov, V. D. Toneev, and A. A. Soldatov, *Phys. Rev. C* **100**, 014908 (2019).
- [22] X.-G. Deng, X.-G. Huang, Y.-G. Ma, and S. Zhang, *Phys. Rev. C* **101**, 064908 (2020), 2001.01371.
- [23] Y. Guo, J. Liao, E. Wang, H. Xing, and H. Zhang, *Phys. Rev. C* **104**, L041902 (2021), 2105.13481.
- [24] A. Ayala, I. Domínguez, I. Maldonado, and M. E. Tejeda-Yeomans, (2021), 2106.14379.
- [25] X.-G. Deng, X.-G. Huang, and Y.-G. Ma, (2021), 2109.09956.
- [26] STAR, T. Niida, *Nucl. Phys. A* **982**, 511 (2019), 1808.10482.
- [27] STAR, J. Adam *et al.*, *Phys. Rev. Lett.* **123**, 132301 (2019), 1905.11917.
- [28] F. Becattini and I. Karpenko, *Phys. Rev. Lett.* **120**, 012302 (2018).
- [29] X.-L. Xia, H. Li, Z.-B. Tang, and Q. Wang, *Phys. Rev. C* **98**, 024905 (2018), 1803.00867.
- [30] X.-L. Xia, H. Li, X.-G. Huang, and H. Z. Huang, *Phys. Rev. C* **100**, 014913 (2019),

- 1905.03120.
- [31] F. Becattini, G. Cao, and E. Speranza, *The European Physical Journal C* **79**, 741 (2019).
 - [32] H. Li, X.-L. Xia, X.-G. Huang, and H. Z. Huang, Global hyperon polarization and effects of decay feeddown, in *19th International Conference on Strangeness in Quark Matter*, 2021, 2108.04111.
 - [33] S. Y. F. Liu, Y. Sun, and C. M. Ko, (2019), 1910.06774.
 - [34] H.-Z. Wu, L.-G. Pang, X.-G. Huang, and Q. Wang, *Nucl. Phys. A* **1005**, 121831 (2021), 2002.03360.
 - [35] H.-Z. Wu, L.-G. Pang, X.-G. Huang, and Q. Wang, *Phys. Rev. Research.* **1**, 033058 (2019), 1906.09385.
 - [36] Voloshin, Sergei A., *EPJ Web Conf.* **171**, 07002 (2018).
 - [37] K. Hattori, M. Hongo, X.-G. Huang, M. Matsuo, and H. Taya, *Phys. Lett. B* **795**, 100 (2019), 1901.06615.
 - [38] K. Fukushima and S. Pu, *Lect. Notes Phys.* **987**, 381 (2021), 2001.00359.
 - [39] K. Fukushima and S. Pu, *Phys. Lett. B* **817**, 136346 (2021), 2010.01608.
 - [40] S. Li, M. A. Stephanov, and H.-U. Yee, *Phys. Rev. Lett.* **127**, 082302 (2021), 2011.12318.
 - [41] D. She, A. Huang, D. Hou, and J. Liao, (2021), 2105.04060.
 - [42] D. Montenegro, L. Tinti, and G. Torrieri, *Phys. Rev. D* **96**, 076016 (2017), 1703.03079.
 - [43] D. Montenegro, L. Tinti, and G. Torrieri, *Phys. Rev. D* **96**, 056012 (2017), 1701.08263, [Addendum: *Phys.Rev.D* 96, 079901 (2017)].
 - [44] W. Florkowski, B. Friman, A. Jaiswal, and E. Speranza, *Phys. Rev. C* **97**, 041901 (2018), 1705.00587.
 - [45] W. Florkowski, E. Speranza, and F. Becattini, *Acta Phys. Polon. B* **49**, 1409 (2018), 1803.11098.
 - [46] F. Becattini, W. Florkowski, and E. Speranza, *Phys. Lett. B* **789**, 419 (2019), 1807.10994.
 - [47] W. Florkowski, R. Ryblewski, and A. Kumar, *Prog. Part. Nucl. Phys.* **108**, 103709 (2019), 1811.04409.
 - [48] D.-L. Yang, *Phys. Rev. D* **98**, 076019 (2018), 1807.02395.
 - [49] S. Bhadury, W. Florkowski, A. Jaiswal, A. Kumar, and R. Ryblewski, (2020), 2002.03937.
 - [50] S. Shi, C. Gale, and S. Jeon, From Chiral Kinetic Theory To Spin Hydrodynamics, in *28th International Conference on Ultrarelativistic Nucleus-Nucleus Collisions (Quark Matter*

- 2019) Wuhan, China, November 4-9, 2019, 2020, 2002.01911.
- [51] A. D. Gallegos, U. Gürsoy, and A. Yarom, (2021), 2101.04759.
- [52] M. Hongo, X.-G. Huang, M. Kaminski, M. Stephanov, and H.-U. Yee, JHEP **11**, 150 (2021), 2107.14231.
- [53] W. Florkowski, B. Friman, A. Jaiswal, R. Ryblewski, and E. Speranza, Phys. Rev. D **97**, 116017 (2018), 1712.07676.
- [54] W. Florkowski, A. Kumar, and R. Ryblewski, Phys. Rev. C **98**, 044906 (2018), 1806.02616.
- [55] W. Florkowski, A. Kumar, R. Ryblewski, and R. Singh, Phys. Rev. C **99**, 044910 (2019), 1901.09655.
- [56] W. Florkowski, A. Kumar, R. Ryblewski, and A. Mazeliauskas, Phys. Rev. C **100**, 054907 (2019), 1904.00002.
- [57] S. Bhadury, W. Florkowski, A. Jaiswal, A. Kumar, and R. Ryblewski, Phys. Rev. D **103**, 014030 (2021), 2008.10976.
- [58] S. Shi, C. Gale, and S. Jeon, Phys. Rev. C **103**, 044906 (2021), 2008.08618.
- [59] R. Singh, G. Sophys, and R. Ryblewski, Phys. Rev. D **103**, 074024 (2021), 2011.14907.
- [60] D.-L. Wang, S. Fang, and S. Pu, (2021), 2107.11726.
- [61] Y.-C. Liu and X.-G. Huang, Nucl. Sci. Tech. **31**, 56 (2020), 2003.12482.
- [62] H.-H. Peng, J.-J. Zhang, X.-L. Sheng, and Q. Wang, (2021), 2107.00448.
- [63] W. Florkowski, R. Ryblewski, R. Singh, and G. Sophys, (2021), 2112.01856.
- [64] P. Copinger and S. Pu, (2022), 2203.00847.
- [65] D.-L. Wang, X.-Q. Xie, S. Fang, and S. Pu, (2021), 2112.15535.
- [66] J.-H. Gao and Z.-T. Liang, Phys. Rev. **D100**, 056021 (2019), 1902.06510.
- [67] N. Weickgenannt, X.-L. Sheng, E. Speranza, Q. Wang, and D. H. Rischke, Phys. Rev. D **100**, 056018 (2019), 1902.06513.
- [68] N. Weickgenannt, E. Speranza, X.-l. Sheng, Q. Wang, and D. H. Rischke, (2020), 2005.01506.
- [69] K. Hattori, Y. Hidaka, and D.-L. Yang, Phys. Rev. **D100**, 096011 (2019), 1903.01653.
- [70] Z. Wang, X. Guo, S. Shi, and P. Zhuang, Phys. Rev. **D100**, 014015 (2019), 1903.03461.
- [71] D.-L. Yang, K. Hattori, and Y. Hidaka, JHEP **07**, 070 (2020), 2002.02612.
- [72] N. Weickgenannt, X.-L. Sheng, E. Speranza, Q. Wang, and D. H. Rischke, Wigner function and kinetic theory for massive spin-1/2 particles, in *28th International Conference on Ultra-relativistic Nucleus-Nucleus Collisions (Quark Matter 2019) Wuhan, China, November 4-9,*

2019, 2020, 2001.11862.

- [73] S. Li and H.-U. Yee, Phys. Rev. **D100**, 056022 (2019), 1905.10463.
- [74] Y.-C. Liu, K. Mameda, and X.-G. Huang, (2020), 2002.03753.
- [75] N. Weickgenannt, E. Speranza, X.-l. Sheng, Q. Wang, and D. H. Rischke, (2021), 2103.04896.
- [76] Z. Wang and P. Zhuang, (2021), 2105.00915.
- [77] X.-L. Sheng, N. Weickgenannt, E. Speranza, D. H. Rischke, and Q. Wang, (2021), 2103.10636.
- [78] A. Huang *et al.*, Phys. Rev. D **103**, 056025 (2021), 2007.02858.
- [79] M. A. Stephanov and Y. Yin, Phys. Rev. Lett. **109**, 162001 (2012), 1207.0747.
- [80] D. T. Son and N. Yamamoto, Phys. Rev. **D87**, 085016 (2013), 1210.8158.
- [81] J.-H. Gao, Z.-T. Liang, S. Pu, Q. Wang, and X.-N. Wang, Phys. Rev. Lett. **109**, 232301 (2012), 1203.0725.
- [82] J.-W. Chen, S. Pu, Q. Wang, and X.-N. Wang, Phys. Rev. Lett. **110**, 262301 (2013), 1210.8312.
- [83] C. Manuel and J. M. Torres-Rincon, Phys. Rev. **D89**, 096002 (2014), 1312.1158.
- [84] C. Manuel and J. M. Torres-Rincon, Phys. Rev. **D90**, 076007 (2014), 1404.6409.
- [85] J.-Y. Chen, D. T. Son, M. A. Stephanov, H.-U. Yee, and Y. Yin, Phys. Rev. Lett. **113**, 182302 (2014), 1404.5963.
- [86] J.-Y. Chen, D. T. Son, and M. A. Stephanov, Phys. Rev. Lett. **115**, 021601 (2015), 1502.06966.
- [87] Y. Hidaka, S. Pu, and D.-L. Yang, Phys. Rev. **D95**, 091901 (2017), 1612.04630.
- [88] Y. Hidaka, S. Pu, and D.-L. Yang, Phys. Rev. **D97**, 016004 (2018), 1710.00278.
- [89] N. Mueller and R. Venugopalan, Phys. Rev. **D97**, 051901 (2018), 1701.03331.
- [90] Y. Hidaka and D.-L. Yang, Phys. Rev. D **98**, 016012 (2018), 1801.08253.
- [91] Y. Hidaka, S. Pu, and D.-L. Yang, Nucl. Phys. **A982**, 547 (2019), 1807.05018.
- [92] J.-H. Gao, Z.-T. Liang, Q. Wang, and X.-N. Wang, Phys. Rev. **D98**, 036019 (2018), 1802.06216.
- [93] A. Huang, S. Shi, Y. Jiang, J. Liao, and P. Zhuang, Phys. Rev. **D98**, 036010 (2018), 1801.03640.
- [94] Y.-C. Liu, L.-L. Gao, K. Mameda, and X.-G. Huang, Phys. Rev. **D99**, 085014 (2019), 1812.10127.
- [95] S. Lin and A. Shukla, JHEP **06**, 060 (2019), 1901.01528.

- [96] S. Lin and L. Yang, Phys. Rev. D **101**, 034006 (2020), 1909.11514.
- [97] N. Yamamoto and D.-L. Yang, Astrophys. J. **895**, 56 (2020), 2002.11348.
- [98] Y. Hidaka, S. Pu, Q. Wang, and D.-L. Yang, (2022), 2201.07644.
- [99] J.-j. Zhang, R.-h. Fang, Q. Wang, and X.-N. Wang, Phys. Rev. C **100**, 064904 (2019), 1904.09152.
- [100] X.-G. Huang, P. Mitkin, A. V. Sadofyev, and E. Speranza, JHEP **10**, 117 (2020), 2006.03591.
- [101] K. Hattori, Y. Hidaka, N. Yamamoto, and D.-L. Yang, JHEP **02**, 001 (2021), 2010.13368.
- [102] S. Lin, (2021), 2109.00184.
- [103] X.-L. Luo and J.-H. Gao, JHEP **11**, 115 (2021), 2107.11709.
- [104] B. Müller and D.-L. Yang, (2021), 2110.15630.
- [105] D.-L. Yang, (2021), 2112.14392.
- [106] S. Y. F. Liu and Y. Yin, Phys. Rev. D **104**, 054043 (2021), 2006.12421.
- [107] S. Y. F. Liu and Y. Yin, JHEP **07**, 188 (2021), 2103.09200.
- [108] F. Becattini, M. Buzzegoli, and A. Palermo, Phys. Lett. B **820**, 136519 (2021), 2103.10917.
- [109] B. Fu, S. Y. F. Liu, L. Pang, H. Song, and Y. Yin, (2021), 2103.10403.
- [110] F. Becattini, M. Buzzegoli, A. Palermo, G. Inghirami, and I. Karpenko, (2021), 2103.14621.
- [111] C. Yi, S. Pu, and D.-L. Yang, Phys. Rev. C **104**, 064901 (2021), 2106.00238.
- [112] X.-Y. Wu, C. Yi, G.-Y. Qin, and S. Pu, (2022), 2204.02218.
- [113] Y. Sun, Z. Zhang, C. M. Ko, and W. Zhao, (2021), 2112.14410.
- [114] Y.-C. Liu and X.-G. Huang, (2021), 2109.15301.
- [115] W. Florkowski, A. Kumar, A. Mazeliauskas, and R. Ryblewski, (2021), 2112.02799.
- [116] F. Becattini, M. Buzzegoli, A. Palermo, and G. Prokhorov, (2020), 2009.13449.
- [117] J.-H. Gao, Phys. Rev. D **104**, 076016 (2021), 2105.08293.
- [118] A. Vilenkin, Phys. Rev. D **22**, 3080 (1980).
- [119] D. E. Kharzeev, L. D. McLerran, and H. J. Warringa, Nucl. Phys. **A803**, 227 (2008), 0711.0950.
- [120] K. Fukushima, D. E. Kharzeev, and H. J. Warringa, Phys. Rev. **D78**, 074033 (2008), 0808.3382.
- [121] D. E. Kharzeev, J. Liao, S. A. Voloshin, and G. Wang, Prog. Part. Nucl. Phys. **88**, 1 (2016), 1511.04050.
- [122] STAR, B. I. Abelev *et al.*, Phys. Rev. Lett. **103**, 251601 (2009), 0909.1739.

- [123] STAR, M. Abdallah *et al.*, (2021), 2109.00131.
- [124] M. Jacob and J. Rafelski, Phys. Lett. B **190**, 173 (1987).
- [125] V. E. Ambrus and M. N. Chernodub, (2019), 1912.11034.
- [126] V. E. Ambrus and M. N. Chernodub, (2020), 2010.05831.
- [127] V. E. Ambrus, JHEP **08**, 016 (2020), 1912.09977.
- [128] R.-h. Fang, J.-y. Pang, Q. Wang, and X.-n. Wang, Phys. Rev. **D95**, 014032 (2017), 1611.04670.
- [129] F. Becattini *et al.*, Eur. Phys. J. C **75**, 406 (2015), 1501.04468, [Erratum: Eur.Phys.J.C 78, 354 (2018)].
- [130] W.-T. Deng and X.-G. Huang, Phys. Rev. **C93**, 064907 (2016), 1603.06117.
- [131] S. M. Mahajan and Z. Yoshida, Phys. Rev. Lett. **105**, 095005 (2010).
- [132] J.-H. Gao, B. Qi, and S.-Y. Wang, Phys. Rev. D **90**, 083001 (2014), 1406.1944.
- [133] Y.-g. Yang and S. Pu, Acta Phys. Polon. Supp. **10**, 771 (2017), 1709.08002.
- [134] J. Wang and S. Pu, Nucl. Phys. Rev. **37**, 679 (2020), 2008.07789.
- [135] L. Pang, Q. Wang, and X.-N. Wang, Phys. Rev. C **86**, 024911 (2012), 1205.5019.
- [136] Z.-W. Lin, C. M. Ko, B.-A. Li, B. Zhang, and S. Pal, Phys. Rev. C **72**, 064901 (2005), nucl-th/0411110.
- [137] P. Huovinen and P. Petreczky, Nucl. Phys. A **837**, 26 (2010), 0912.2541.
- [138] W.-T. Deng and X.-G. Huang, Phys. Rev. **C85**, 044907 (2012), 1201.5108.
- [139] V. Roy and S. Pu, Phys. Rev. **C92**, 064902 (2015), 1508.03761.
- [140] Y. Jiang, Z.-W. Lin, and J. Liao, Phys. Rev. **C94**, 044910 (2016), 1602.06580, [Erratum: Phys. Rev.C95,no.4,049904(2017)].
- [141] W.-T. Deng and X.-G. Huang, Phys. Rev. C **93**, 064907 (2016), 1603.06117.
- [142] STAR, J. Adam *et al.*, Phys. Rev. **C98**, 014910 (2018), 1805.04400.
- [143] J. R. Adams and M. A. Lisa, (2021), 2109.14726.